Microscopic structure of charge-exchange spin-isospin modes through decay measurements

Harakeh, M.N.

MICROSCOPIC STRUCTURE OF CHARGE-EXCHANGE SPIN–ISOSPIN MODES THROUGH DECAY MEASUREMENTS*

M.N. Harakeh

Kernfysisch Versneller Instituut
Zernikelaan 25, 9747 AA Groningen, The Netherlands

The study of particle decay of charge-exchange giant resonances (CEGR) furnishes information on their microscopic structure. Furthermore, γ decay of CEGR can help to unravel their structure. For example, the γ-decay of the Gamow–Teller (GT) resonance to the isobaric analogue state (IAS) points to a possible method to study quenching of GT strength. The study of γ-decay of the spin-flip dipole resonance (SDR) to GT and low-lying states will possibly allow to disentangle the different spin components. These aspects will be discussed in the light of recent $(^3\mathrm{He},t)$ experiments at $\mathrm{E}(^3\mathrm{He}) = 450$ MeV and $\theta = 0°$ performed to study the proton decay of CEGR in ^{208}Bi and ^{12}N and the γ decay of the GT resonance, IAS and SDR in ^{90}Nb.

PACS numbers: 21.60.–n, 25.55.Kr

1. Introduction

The charge-exchange giant resonances (CEGR) populated in (p, n)-type and (n, p)-type reactions have 1-proton-particle–1-neutron-hole ($1\pi\mathrm{p}$–$1\nu\mathrm{h}$) and 1-neutron-particle–1-proton-hole ($1\nu\mathrm{p}$–$1\pi\mathrm{h}$) collective configurations, respectively. Therefore, the study of the particle decay of these CEGR via proton and neutron decay to neutron-hole and proton-hole states, respectively, furnishes information on their microscopic structure. Furthermore, γ decay of the CEGR to low-lying states, though expected to be small and very difficult to study experimentally, can help to unravel their structure. The γ-decay of the Gamow–Teller (GT) resonance to the isobaric analogue state (IAS) points to a possible method to study the quenching of GT strength.

The quenching should be reflected in the γ-decay matrix elements because of the coherence of the IAS which exhausts almost 100% of the sum rule for Fermi transitions. The study of γ-decay of the spin-flip dipole resonance (SDR) to GT and low-lying states can shed light onto the coupling of the 1p–1h SDR to 2p–2h configurations and allow the disentangling of the various SDR spin components, *i.e.* the $0^-, 1^-$ and 2^- components.

The charge-exchange modes, which can be described as a coherent superposition of 1πp–1νh configurations, lend themselves easily for experimental investigation of their microscopic structure by studying their proton decay. The $(^3\text{He},tp)$ reaction is very suitable for such studies because of the 100% detection efficiency of the tritons and also the good total energy resolution that can be achieved with a magnetic spectrometer. At intermediate energies (≥ 100 MeV/u), the preferential excitation of spin-isospin-flip modes in the $(^3\text{He},t)$ reaction [1] allows, in conjunction with proton decay, the study of the microscopic structure of these modes and in particular the Gamow-Teller resonance (GTR) [2, 3] and the spin-flip ΔL=1 resonances (SDR) [4].

The charge-exchange modes, which can be described as a coherent superposition of 1νp–1πh configurations, lend themselves less easily for experimental investigation, because they are excited by (n, p)-type reactions. These are usually difficult to perform with neutron beams because of their low intensities necessitating the use of thick targets and thus resulting in worse energy resolution. This furthermore practically rules out decay studies because of the expected low counting rates. These CEGR were recently studied with the $(d,^2\text{He})$ reaction with much success in spite of the experimental difficulties and complicated data analysis of this reaction. The spin selectivity (ΔS $= 1$) of this reaction and the reasonably high detection efficiency that can be achieved allow even the study of neutron decay of these CEGRs [5]. The GT resonance (GTR) required to explain the missing GT strength in β-decay [2, 3] was discovered in studies of the (p, n) charge-exchange reaction at intermediate bombarding energies. The fraction of the GT sum rule exhausted by the GTR was obtained by normalizing to sum-rule strength of a low-lying transition, for which the GT matrix element is known from β-decay measurements. This is based on the proportionality of the $0°$ (p, n) GTR and IAS cross sections to the B(GT) and B(F) reduced transition rates, respectively [6, 7]. In this way, it was found [8] that the GTR depletes $\simeq 60\%$ of the GT sum rule as a function of mass number. In attempting to explain this quenching two mechanisms were proposed [9]: *(i)* the coupling to the Δ excitation in the nucleus and/or *(ii)* the coupling to high-lying 2p–2h configurations through the tensor interaction. Recent experimental evidence indicates that the second mechanism, *i.e.* coupling to high-lying 2p–2h configurations, is responsible for the depletion of strength in the GTR region [10].

A possible method [11] to study the quenching of the GT strength is by studying the γ-decay of the GTR to the IAS. In a simple schematic model, the GT and IAS belong to the same Wigner supermultiplet [12] with similar wave functions that differ only by the spin-flip components. Therefore, the GTR should be connected to the IAS by coherent M1 γ-decay, which can be calculated quite accurately since the M1 operator is well known, and involves in addition to the spin-flip component also an orbital part:

$$\hat{O}(M1) = \sqrt{\frac{3}{4\pi}} \sum_i \left(g_{s_i} \vec{s}_i + g_{l_i} \vec{l}_i \right).\tag{1}$$

By comparing the measured B(M1) reduced transition rate to the calculated one, assuming the GTR exhausts 100% of the GT sum rule, one can extract the quenching factor in a somewhat less model-dependent way than from the (p, n) reaction.

Recently, Sagawa *et al.* [13] considered the magnetic-dipole transition rates connecting GT states to the IAS. Based on non-energy-weighted sum-rule arguments they showed that M1 transitions between GT states and IAS are enhanced by factors as large as ~ 2.5 compared to their analogues in the parent nucleus. Furthermore, the authors calculated M1 transition strength between IAS and specific GT states using the Tamm-Dancoff approximation (TDA) in a 1p–1h shell-model space. The results show large M1 transition strengths between several of these states and the IAS suggesting that measurements of these M1 decays may be feasible.

In the following, results of some experiments performed [5,14,15] recently at RCNP, Osaka will be discussed.

2. Experimental procedure and data analysis

The ^{208}Pb(^{3}He,tp) and ^{12}C(^{3}He,tp) experiments have been described in detail in Ref. [14] and Ref. [5], respectively, and the ^{90}Zr(^{3}He,$t\gamma$) in Ref. [15]. Here, only the salient features of these experiments will be described.

In all of the experiments, a 450 MeV ^{3}He^{++} beam extracted from the ring cyclotron of the RCNP, Osaka was used to bombard isotopically enriched targets (^{208}Pb, ^{12}C and ^{90}Zr, respectively). Typical beam intensities were 2-5 nA. The ejectile tritons were detected in the spectrometer Grand Raiden [16], which was set at 0° with vertical and horizontal opening angles of 40 mrad each. The ^{3}He^{++} beam was fully intercepted by a Faraday cup in the first dipole magnet.

The ejectile tritons were detected with the focal-plane detection system which allows the reconstruction of the horizontal and vertical scattering angles at the target by ray-tracing techniques with uncertainties of less than

2 mrad and 10 mrad, respectively. Because of the characteristic angular distributions of the IAS, GTR and spin-flip $\Delta L=1$ resonances at angles near $0°$, software cuts on the deduced scattering angles can be used to enhance the relative contributions of these resonances in the spectra.

The proton decay of CEGR in ^{208}Bi and ^{12}N to the low-lying states in ^{207}Pb and ^{11}C, respectively, was measured with Si(Li) solid-state detectors (SSD). In the ^{208}Bi and ^{12}N experiments, 8 and 40 SSDs were used, respectively. These were set in an azimuthally symmetric configuration at backward angles with respect to the incident ^{3}He beam direction. Setting the SSDs at backward angles is necessary to avoid detection of protons due to the quasi-elastic charge-exchange knock-on process and the breakup/pickup process at forward angles.

Two-dimensional scatter plots of proton energies measured versus the excitation energies in ^{208}Bi are given in Ref. [14] and the ones for ^{12}N, shown in Fig. 1, were generated in a similar procedure. The final-state spectrum for ^{12}N decay, also shown in Fig. 1, was obtained by projecting the two-dimensional scatter plot. Decay to the final states $\frac{3}{2}^{-}$, $g.s.$, $\frac{1}{2}^{-}$, $\frac{5}{2}^{-}$, $\frac{3}{2}^{-}$, and $\frac{1}{2}^{+}$ states as well as to the $\frac{1}{2}^{-}$ state at 8.1 MeV in ^{11}C is quite evident. The total resolution of the proton and triton sum energy was about 400 keV in both experiments. This was not sufficient to completely resolve the decay to the 1st and 2nd excited states of ^{207}Pb and 2nd and 3rd excited states in ^{11}C.
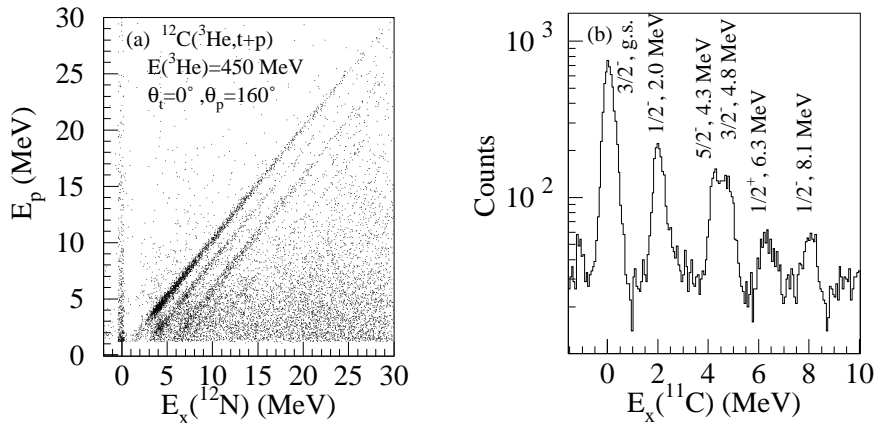
Fig. 1. (a) — two-dimensional scatter plot of proton-triton coincidence events induced by the ^{12}C(^{3}He,t) reaction at $\theta \sim 0°$. The loci indicate proton decay to final states in ^{11}C. Proton events with energies lower than $\sim$1.2 MeV are cut off by an electronic threshold. (b) — the final-state spectrum of ^{11}C obtained by projecting loci in the scatter plot onto the excitation energy axis of ^{11}C.

The γ-ray decay of the low-lying states, IAS, GTR and SDR in ^{90}Nb was measured in coincidence with tritons in six 3" ø × 6" NaI crystals which were mounted in an axially symmetric configuration around the beam direction. The crystals were set at a backward angle of $\theta = 120°$ and at a distance of about 10 cm from the target.

Two-dimensional scatter plots of γ-ray energy measured in NaI detectors versus triton energy [or excitation energy in ^{90}Nb] were generated for prompt and random events by gating on prompt and random peaks in the time spectra. Because the NaI detectors are of medium size and have not been provided by an anti-coincidence shield, the γ-ray response and the photo-peak efficiency vary strongly as a function of γ-ray energy. Therefore, to distinguish the loci for γ-ray decay the response of the NaI detectors has to be unfolded.
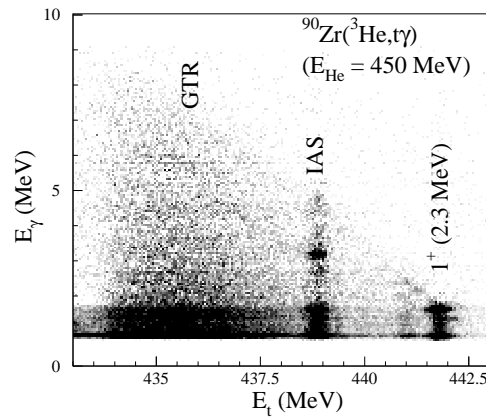

Fig. 2. Two-dimensional scatter plot of γ-ray energy versus triton energy obtained at E(^{3}He) = 450 MeV and $\theta_t = 0°$ is shown for the excitation energy region below the neutron decay threshold in ^{90}Nb and after unfolding the response of the NaI detectors. The loci for γ decay to the 2^+ state at 0.85 MeV and 1^+ state at 2.3 MeV are visible.

In Fig. 2, a 2-dimensional scatter plot of γ-ray energy after unfolding the response of the NaI detector is shown versus triton energy for the region of excitation energy from the GTR down to the 1^+ state at 2.3 MeV. Loci of γ-ray decay to low-lying states can now be identified in the spectrum. Unfortunately, the most interesting γ-decay branch for this study, *i.e.* γ-decay from the GTR to the IAS, can not be well identified. The background counts due to statistical γ-ray decay of the GTR are relatively high compared to γ-transitions from GTR to IAS. This is compounded by the not very favourable overall resolution obtained for the sum spectrum (E$_t$ + E$_\gamma$) of between 400 and 600 keV mainly due to beam resolution. This is clearly not sufficient to enhance this locus above the background events.

3. Results and discussion

3.1. Proton decay of CEGR in ^{208}Bi

In this experiment, which is described in detail in Ref. [14], the resonance energies and total widths of the GTR and SDR were determined by decomposing the singles spectra. The resonance energy and total width of the GTR were determined from this decomposition to be: E = 15.6 ± 0.2 MeV and Γ = 3.72 ± 0.25 MeV, respectively. For the SDR these were: E = 21.1 ± 0.8 MeV and Γ = 8.4 ± 1.7 MeV.

The partial proton escape widths of the IAS and the GTR in ^{208}Bi to the $3p_{1/2}$, $2f_{5/2}$, $3p_{3/2}$, and $2f_{7/2}$ neutron-hole states in ^{207}Pb were determined from the measured branching ratios. The latter were determined from the peak areas of the IAS and GTR in the spectra which are obtained by gating on the various final hole states in ^{207}Pb. For the GTR the proton escape widths are given in column 5 of Table I. Since the resolution was not sufficient to separate the decay to the $2f_{5/2}$ and $3p_{3/2}$ neutron-hole states in ^{207}Pb, the sum of the partial decay widths is given.

TABLE I

Experimental and theoretical partial and total (escape) proton widths, $\Gamma^{\uparrow}_{p_i}$ and $\Sigma_i\Gamma^{\uparrow}_{p_i}$, for the decay of the GTR in ^{208}Bi into neutron-hole states in ^{207}Pb.

neutron-hole states in ^{207}Pb	E_x [keV]	theor[a] [keV]	theor[b] [keV]	exp[c] [keV]
$3p_{1/2}^{-1}$	0	66	60.8	58.4 ±19.8
$2f_{5/2}^{-1}$	570	90	54.0	incl. in $p_{3/2}$
$3p_{3/2}^{-1}$	898	99	50.5	101.5 ±31.3
$1i_{13/2}^{-1}$	1633	3	0.73	8.3 ±9.4
$2f_{7/2}^{-1}$	2340	15	5.95	15.6 ±7.6
$1h_{9/2}^{-1}$	3413	3	0.19	
total		276	172.7	184 ±49

[a] Obtained in TDA with SIII interaction and taking proton escape energies and neutron spectroscopic factors from experiment [17].
[b] Obtained in RPA (Refs. [18, 19]) and taking neutron spectroscopic factors from experiment.
[c] Present experimental results; see also Ref. [14].

Results of recent calculations by Coló *et al.* [17] and the Moscow group [18, 19] are given in Table I. Coló *et al.* calculated the various characteristics of the GTR in TDA with explicit coupling to the continuum. The results

obtained with the SIII Skyrme force and employing the experimental proton escape energies and spectroscopic factors for neutron pickup from ^{208}Pb are given in column 3 and show reasonable agreement with the experimental results. Better agreement with the experimental results is obtained by the Moscow group in RPA with coupling to the continuum. In these calculations the experimental spectroscopic factors are used (column 4).

For the decay of the SDR in ^{208}Bi, the partial proton escape widths to the various neutron-hole states in ^{207}Pb have not been determined nor have the various spin components (2^-, 1^- and 0^-) of the SDR been disentangled using their angular correlation patterns. However, one can infer from the final-state spectra (not shown here) that the population pattern of the various neutron-hole states is different for the SDR than for the GTR, in that the $1i_{13/2}$ and $2f_{7/2}$ are more strongly and the $3p_{1/2}$ more weakly populated. Furthermore, the total proton decay branching ratio has been determined from the coincidence spectra to be $14.1 \pm 4.2\%$. If assumed to be due to decay of one single resonance with a width of 8.4 ± 1.7 MeV, this would lead to a total proton escape width of 1.18 ± 0.35 MeV. It is interesting to note that the Moscow group, in the same calculation in which they reproduced the results for the GTR [19], obtained a branching ratio of 16.1% and a total proton escape width of 1.35 MeV for the SDR in very good agreement with our results.

The SDR bump consists of three spin components, *i.e.* 2^-, 1^- and 0^-. Even if one considers that the total proton escape width determined above should be divided among these three components, the resulting proton escape width per component is still considerably larger than for the GTR. This has to do with the increase of the proton energy available above the Coulomb barrier and also the average decrease of the angular-momentum barrier for the decay protons as compared to the GTR. Indications also appear for proton decay to the $1h_{9/2}$ broad neutron deep-hole state in ^{207}Pb.

3.2. Proton decay of CEGR in ^{12}N

In Fig. 3, a ^{12}C(^{3}He,t)^{12}N singles spectrum taken at $\theta = 0°$ is shown. In order to get the angular correlations of proton decay the bump structure and the continuum region were divided into different bins as indicated.The strongly excited peak at $E_x = 4.1$ MeV in ^{12}N is known to be mainly due to a 2^- state although a small peak due to a 4^- state, which is excited with a weak intensity at $\theta = 0°$ [20], could be present. The resonance region denoted by A ($E_x = 3.0{\sim}5.0$ MeV) in Fig. 3 is further divided into two bins A1 ($E_x = 3.5{\sim}4.5$ MeV) and A2 ($E_x = 4.5{\sim}5.0$ MeV), and the angular correlations (not shown here) are obtained for each region. The present experiment shows that the angular correlations for proton decay from the
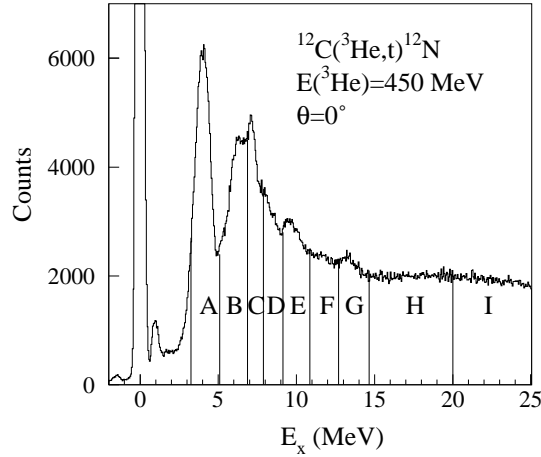
Fig. 3. A singles spectrum at $\theta = 0°$ for the ^{12}C(^{3}He,t)^{12}N reaction at $E(^3$He)=450 MeV. The regions denoted as A–I indicate the gating bins for which angular-correlation patterns for proton decay into the final states in ^{11}C have been determined.

subdivided regions A1 and A2 are not the same. In the present (^{3}He,t) measurement at 450 MeV and $\theta \approx 0°$, admixtures of the 3^- and 4^- states are expected to be small. This indicates that two levels of low multipolarity but different structure contribute to the 4.1 MeV broad peak. This may further explain the fact that the observed width of 1.36 MeV in the present experiment is much larger than the 0.83 MeV width reported by Ref. [21] for the 2^- state at 4.1 MeV.

In the regions B and C corresponding to the 7 MeV resonance in ^{12}N, the angular-correlation patterns for decay to the $\frac{3}{2}^-$, ground state of ^{11}C are essentially similar to those for the 4.1 MeV, 2^- resonance decay. The observed resonance at $E_x \sim 7$ MeV in the ^{12}C(^{3}He,t)^{12}N singles spectrum (see Fig. 3) obviously consists of many peaks: there are many structures including a sharp peak at 7.1 MeV. This suggests that in the 7 MeV region, there are several states possibly consisting of 1^- and 2^- states and other states with a mixture of spin-flip and non-spin-flip natures. This is consistent with the shell-model predictions [20]. Experimentally, it is difficult to extract the distributions of spin-flip and non-spin-flip strengths for the $\Delta L = 1$ transitions.

Fig. 4 shows the coincidence spectra gated on proton decay to the $1p_{3/2}^{-1}$, $\frac{3}{2}^-$ ground state, the first $\frac{1}{2}^-$ state, and to the first $\frac{5}{2}^-$ and second $\frac{3}{2}^-$ states in ^{11}C. One can clearly observe different populations from the intermediate resonances in ^{12}N to these final states in ^{11}C. The broad resonance at 4.1
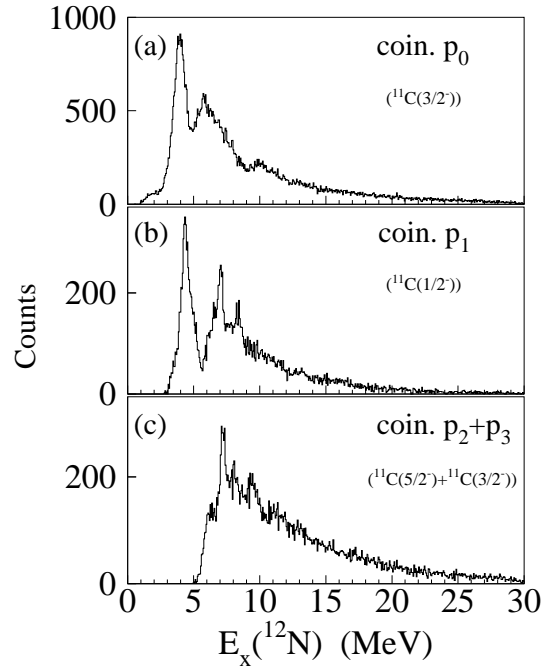
Fig. 4. Coincidence ^{12}C(^{3}He,tp) spectra gated on proton decay to (a) the $\frac{3}{2}^-$, *g.s.*, (b) the first $\frac{1}{2}^-$ state, and to the first $\frac{5}{2}^-$ and second $\frac{3}{2}^-$ states in ^{11}C.

MeV seems to split into two resonances: one decaying to the $\frac{3}{2}^-$ ground state of ^{11}C (Fig. 4(a)), and the higher one to the $\frac{1}{2}^-$ first-excited state (Fig. 4(b)). Considering that at these low decay energies for protons, $l = 0$ decay will be favoured compared to $l = 2$ decay, since in the latter case, protons will have to penetrate both the Coulomb and centrifugal barriers, it appears that the lower resonance peak corresponds to a 2^- state and the higher one to a 1^- state. This observation that two resonances may be involved in the 4.1 MeV bump is in agreement with the results from the angular correlations measured for regions A1 and A2, and is also consistent with the observation of the larger width in the present (^{3}He,t) measurement mentioned above.

The decay patterns from the 7 MeV resonance in ^{12}N to the $\frac{3}{2}^-$ ground state (Fig. 4(a)), the first $\frac{1}{2}^-$ state (Fig. 4(b)), and to the first $\frac{5}{2}^-$ and second $\frac{3}{2}^-$ states (Fig. 4(c)) also differ from each other. A clear peak corresponding to the 6.4 MeV peak seen in region B in Fig. 3 is also identified in Fig. 4(a). However, the same peak disappears in Fig. 4(b). This suggests that the resonance at 6.4 MeV (denoted by region B in Fig. 3) mainly decays into the $\frac{3}{2}^-$ ground state in ^{11}C. On the other hand, the sharp peak at 7.1 MeV

is not observed in the spectrum gated on proton decay to the $\frac{3}{2}^-$ ground state in ^{11}C. Instead, the 7.1 MeV state strongly populates the first $\frac{1}{2}^-$ state, and the first $\frac{5}{2}^-$ and second $\frac{3}{2}^-$ states. These observations indicate different microscopic structures for the two resonances at 6.4 and 7.1 MeV.

In the $7.9 < E_x(^{12}$N$) < 10.9$ MeV region (D and E regions in Fig. 3), there is a sharp state at ∼8.4 MeV, which is clearly identified in both spectra gated on proton decays to the first $\frac{1}{2}^-$ state and to the first $\frac{5}{2}^-$ and second $\frac{3}{2}^-$ states in ^{11}C. There is another peak observed at ∼9.5 MeV, which is rather broad ($\Gamma \approx 0.7$ MeV) and is observed only in the spectra gated on proton decays to the the first $\frac{5}{2}^-$ and second $\frac{3}{2}^-$ states (see Fig. 4(c)).

In the theoretical calculation of Gillet and Vinh Mau [22], a 0^- state is predicted in the region of $9.1 < E_x(^{12}$N$) < 10.9$ MeV (region E). Actually, we observed a clear bump at 9.9 MeV. If the bump corresponds to the 0^- state, the angular correlation should be isotropic. Our experimental results show that the angular-correlation pattern (not shown here) is not isotropic, but is similar to that of the 7 MeV resonance. Thus, we can not find any evidence for the presence of the 0^- state in this excitation energy region. The resonance at 9.9 MeV strongly decays by proton emission into the $\frac{3}{2}^-$ ground state in ^{11}C. The bump is clearly observed in the spectrum gated with proton decay to the $\frac{3}{2}^-$ ground state as shown in Fig. 4(a), but can not be identified in Figs. 4(b) and (c).

3.3. Gamma decay of CEGR in ^{90}Nb

The calculation of magnetic dipole (M1) transitions between GT states and IAS by Sagawa *et al.* [13] showed that these transitions occur with sizeable enhancements and therefore could provide additional information on the quenching issue of GT strength. The enhancement factors, κ, for the M1 transition strength between IAS and GT states can be easily calculated for closed-subshell nuclei. The enhancement factor for ^{90}Nb is large leading to an increase in the M1 strength by a factor of ∼ 2.5. There is, however, a hindrance factor due to the fact that the GTR is obtained within a 1p–1h space, whereas the large enhancement originates from the 1^+ states in 2p–2h space (see Ref. [13]). After correcting for this hindrance factor, the enhancement of M1 transitions between IAS and GT states in ^{90}Nb is still large of ∼ 2.

In spite of the predicted enhancement for M1 transitions between IAS and GT states, we have unfortunately not been able, as stated above, to identify the γ-decay of the GTR to the IAS. Essentially, this decay is embedded within the statistical γ decay of the GTR and needs a high overall $(E_t + E_\gamma)$ resolution to isolate it and accurately determine it. we have in-

stead found clear evidence for γ-ray decay from the GTR to low-lying 1^+ and 2^+ states with the configuration $[1\pi g_{9/2}1\nu g_{9/2}^{-1}]$. This is rather interesting because the main component of the wave function of the GTR has a configuration $[1\pi g_{7/2}1\nu g_{9/2}^{-1}]$. The transitions should thus be mainly M1. In this respect, it is worthy to note that the IAS, which also has the main configuration $[1\pi g_{9/2}1\nu g_{9/2}^{-1}]$, decays by γ emission to the same 1^+ and 2^+ states. However, to determine the branching ratios for a comparison of the decay of the IAS with the theoretical calculations the absolute γ-ray detection efficiency of the NaI detectors need to be determined.

The observed γ decay of the GTR and IAS to low-lying 1^+ and 2^+ states deserves further study both theoretically and experimentally. Theoretically, the M1 decay of the GTR to the IAS has been calculated [13] but also its M1 decay to low-lying 1^+ and 2^+ states is needed. Similarly, the M1 decay of the IAS to low-lying 2^+ states needs to be calculated. Experimentally, one needs to determine the partial decay widths absolutely and with good accuracy. This needs yet to be worked out. However, the more interesting M1 γ decay from the GTR to the IAS will remain elusive unless much better final-state resolution of $\simeq 200$ keV or less and with high γ-ray detection efficiency can be achieved. In that case, also the γ-decay from the spin-flip ΔL=1 resonances may possibly be determined simultaneously. This will furnish information which will shed light onto the coupling of the 1p–1h collective SDR to 2p–2h configurations [23] and hopefully enable us to discriminate the various J^π components, *i.e.* 0^-, 1^- and 2^-. Such an experiment has been undertaken recently at KVI wherein a HPGe clover detector and a large NaI detector (10" ø × 14") were used to detect the γ-rays. The overall energy resolution of the final-state spectrum is determined by the beam energy resolution and is found to be better than 300 keV. The data analysis of this experiment is underway.

REFERENCES

[1] I. Bergqvist *et al.*, *Nucl. Phys.* **A469**, 669 (1987), and references therein.

[2] K. Ikeda, S. Fujii, J. I. Fujita, *Phys. Lett.* **3**, 271 (1963).

[3] J. I. Fujita, K. Ikeda, *Nucl. Phys.* **67**, 145 (1965).

[4] H. Ejiri, K. Ikeda, J. I. Fujita, *Phys. Rev.* **176**, 1277 (1968).

[5] T. Inomata *et al.*, *Phys. Rev.* **C57**, 3153 (1998), and references therein.

[6] C. D. Goodman *et al.*, *Phys. Rev. Lett.* **44**, 1755 (1980).

[7] T. N. Taddeucci *et al.*, *Nucl. Phys.* **A469**, 125 (1987), and references therein.

[8] C. Gaarde, in *Weak and Electromagnetic Interactions in Nuclei*, ed. H. V. K. Klapdor, Springer-Verlag, Berlin 1986, p. 260.

[9] F. Osterfeld, *Rev. Mod. Phys.* **64**, 491 (1992).

[10] T. Wakasa *et al.*, *Phys. Rev.* **C55**, 2909 (1997).

[11] M. N. Harakeh *et al.*, Research proposal to RCNP for a study of the γ decay of the Gamow-Teller Resonance in ^{90}Nb (1993/1994).

[12] E. P. Wigner, *Phys. Rev.* **51**, 106 (1937); *Phys. Rev.* **56**, 519 (1939).

[13] H. Sagawa, T. Suzuki, Nguyen Van Giai, *Phys. Rev. Lett.* **75**, 3629 (1995).

[14] H. Akimune *et al.*, *Phys. Rev.* **C52**, 604 (1995).

[15] M. N. Harakeh *et al.*, in *Nuclear Reaction Dynamics of Nucleon-Hadron Many Body System*, eds. H. Ejiri, T. Noro, K. Takahisa, H. Toki, World Scientific, Singapore 1996, p. 169.

[16] M. Fujiwara *et al.*, in Proc. 5th French–Japanese Symposium on Nuclear Physics, Dogashima, Japan, September 26–30 (1989), p. 348.

[17] G. Coló *et al.*, *Phys. Rev.* **C50**, 1496 (1994), and references therein.

[18] S. E. Muraviev, M. G. Urin, *Nucl. Phys.* **A572**, 267 (1994).

[19] E. A. Moukhai, V. A. Rodin, M. H. Urin, preprint.

[20] B. D. Anderson *et al.*, *Phys. Rev.* **C54**, 237 (1996).

[21] F. Ajzenberg-Selove, *Nucl. Phys.* **A506**, 1 (1990).

[22] V. Gillet, N. Vinh Mau, *Nucl. Phys.* **54**, 321 (1964).

[23] T. Suzuki, H. Sagawa, Nguyen Van Giai, *Phys. Rev.* **C57**, 139 (1998).